Kinematic Calibration of Delta Robot using Distance Measurements

Pujun Bai, Jiangping Mei, Tian Huang*

Key Laboratory of Mechanism Theory and Equipment Design of The State Ministry of Education

Tianjin University, Tianjin 300072, China

Derek G. Chetwynd

School of Engineering, The University of Warwick, Coventry CV4 7AL, UK

Abstract

This paper deals with kinematic calibration of the Delta robot using distance measurements. The work is mainly placed upon: (1) the error modeling with a goal to classify the source errors affecting both the compensatable and uncompensatable pose accuracy; (2) the full/partial source error identification using a set of distance measurements acquired by a laser tracker; and (3) design of a linearized compensator for real-time error compensation. Experimental results on a prototype show that positioning accuracy of the robot can significantly be improved by the proposed approach.

Keywords: Delta robot, Geometric error modeling, Kinematic calibration

1. Introduction

Geometric accuracy is an important performance index of parallel mechanisms. It has been well recognized that the kinematic calibration is a practical and economical way for enhancing the pose accuracy of parallel mechanisms provided that adequate fundamental precision can be achieved at manufacturing and assembly level. The calibration process can be implemented by four sequential steps, i.e. modelling, measurement, identification and implementation [1-4] such that the kinematic model residing in the controller more closely matches the real system.

Since the measurement is time and cost consuming, laborious and prone to human errors, the kernel step in the calibration is to identify the geometric parameters in such a way that measurements can easily be made in a time and cost effective manner without compromising the accuracy of the end results. In the past few decades, intensive studies have been carried out for kinematic calibration of parallel mechanisms and the approaches available to hand can be classified into two categories. One category is regarded as the external calibration [5-9] as the geometric parameters are identified by

* Corresponding author, email: tianhuang@tju.edu.cn

minimizing the residuals between the measured and computed values of the external pose sensors. Another category is referred to as the self or autonomous calibration [10-13] since the parameter identification is implemented by minimizing the discrepancies between the measured and computed values of the active, passive and/or redundant joint sensors. As for the external calibration the further classification can be made into the coordinate base approach [5, 7] and the distance based approach [9, 10], heavily dependent upon the metrology devices being used. The coordinate based approach deals with the identification problem using the full/partial set of position/orientation coordinate measurements. The distance or 1-dimensional based approach deals with the same problem using a set of distance measurements either directly achieved by a metrology device, a double ball bar for example, or extracted from the absolute coordinates of one or more reference points on the end-effector. Compared with the coordinate based approach, the advantages of the distance based approach lies in that it is invariant with the reference frame chosen and it is unnecessary to identify the source errors describing the rigid body motion of robot frame relative to the world frame because robot localization can be carried out late on according to the environment context.

Building mainly upon the first order approximation, this paper deals with kinematic calibration of the Delta robot [14] using distance-based approach. Although this problem were intensively studied using the autonomous or coordinate-based approach [6-8, 15-17] in the past, we will focus upon: (1) geometric error modeling by classifying the source errors affecting the compensatable and uncompensatable pose accuracy; (2) identifiability analysis of the source errors affecting the uncompensatable pose accuracy; and (3) development of a linear error compensator for the real-time implementation. Experiments will be carried out on a prototype to validate the effectiveness of this approach.

2. Error Modelling

Fig.1 shows a 3-D view of a Delta robot which is composed of a base, a traveling plate, and three identical $\underline{R}$-$(SS)^2$ limbs. Here, $\underline{R}$ represents a actuated revolute joint connected with the base, $(SS)^2$ denotes two spherical joints at either extremity of a spatial parallelogram. In order to formulate the error model containing all possible geometric source errors, the following points and frames are defined as shown in Fig. 2.

$C_{j,i}$ ($A_{j,i}$): Centre point of the jth S-joint attached to the proximal link (traveling plate) in the ith limb.

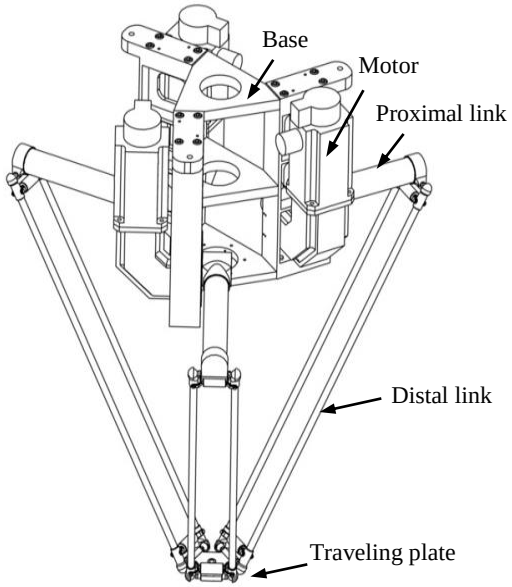

Fig.1 A 3-D view of the Delta robot

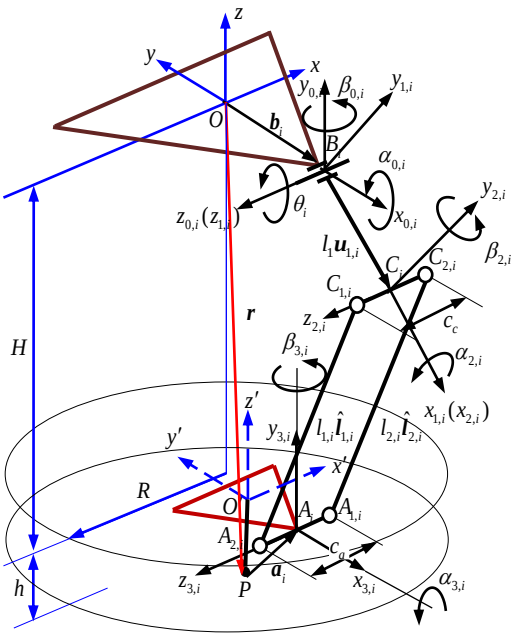

Fig. 2 Schematic diagram of a limb in the Delta robot

C_i (A_i): Middle point of $\overrightarrow{C_{1,i}C_{2,i}}$ ($\overrightarrow{A_{1,i}A_{2,i}}$):

B_i : Projection of C_i onto the rotational axis of the R-joint in the ith limb

$\{O\}$: Reference frame attached to the base

$\{O'\}$: Body fixed frame attached to the travelling plate

$\left\{{}^{0}B_i\right\}$: Reference frame of the ith limb with $z_{0,i}$ being the rotational axis of the R-joint

$\left\{{}^{1}_{0}B_i\right\}$: Body fixed frame of the ith proximal link achieved by rotating $\left\{{}^{0}B_i\right\}$ an angle about the $z_{0,i}$ axis

$\left\{{}^{2}_{1}C_i\right\}$: Body fixed frame of the ith proximal link with the direction of $\overrightarrow{C_{1,i}C_{2,i}}$ being the $z_{2,i}$ axis

$\left\{{}^{3}_{0'}A_i\right\}$: Body fixed frame of the travelling plate with the direction of $\overrightarrow{A_{1,i}A_{2,i}}$ being the $z_{3,i}$ axis

Considering that the source errors are much smaller than their normal values, the first order approximation of the jth loop closure vector equation within the ith limb can be formulated by

$$\begin{aligned}\Delta\boldsymbol{r} = {} & \Delta\boldsymbol{e}_i + \Delta L_i\boldsymbol{u}_{1,i} + \boldsymbol{R}_{0,i}\left(\Delta\boldsymbol{\theta}_{0,i} + \Delta\boldsymbol{\theta}_{1,i}\right)\times L\boldsymbol{u}_{1,i} + \frac{1}{2}\mathrm{sgn}(j)\Delta c_{c,i}\boldsymbol{w}_{0,i} + l\Delta\boldsymbol{\varepsilon}_{j,i}\times\hat{\boldsymbol{l}}_i \\ & + \Delta l_{j,i}\hat{\boldsymbol{l}}_i + \boldsymbol{R}_{0,i}\left(\Delta\boldsymbol{\theta}_{0,i} + \Delta\boldsymbol{\theta}_{1,i} + \boldsymbol{R}_{1,i}\Delta\boldsymbol{\theta}_{2,i}\right)\times\frac{1}{2}\mathrm{sgn}(j)c\boldsymbol{w}_{0,i} - \frac{1}{2}\mathrm{sgn}(j)\Delta c_{a,i}\boldsymbol{w}_{0,i} \\ & - \left(\Delta\boldsymbol{\varepsilon} + \boldsymbol{R}_{3,i}\Delta\boldsymbol{\theta}_{3,i}\right)\times\frac{1}{2}\mathrm{sgn}(j)c\boldsymbol{w}_{0,i} - \Delta\boldsymbol{\varepsilon}\times\boldsymbol{a}_i\end{aligned} \tag{1}$$

$$i = 1,2,3;\ \ j = 1,2,\ \ \mathrm{sgn}(j) = \begin{cases} 1 & j = 1 \\ -1 & j = 2 \end{cases}$$

with descriptions of the following scalars, vectors and matrices:

$L,\ l,\ c$: the nominal lengths of the proximal link, distal link and $\overrightarrow{C_{1,i}C_{2,i}}$ ($\overrightarrow{A_{1,i}A_{2,i}}$), and ΔL_i , $\Delta l_{j,i}$, $\Delta c_{c,i}(\Delta c_{a,i})$ are their errors;

$\hat{\boldsymbol{l}}_i$: the nominal unit vector of the distal links in the ith limb

$\boldsymbol{a}_i = (a_{x,i} \quad a_{y,i} \quad a_{z,i})^{\mathrm{T}}$: the nominal position vector of A_i evaluated in $\{O'\}$

$\boldsymbol{b}_i = (b_{x,i} \quad b_{y,i} \quad b_{z,i})^{\mathrm{T}}$: the nominal position vector of B_i evaluated in $\{O\}$

$\boldsymbol{R}_{0,i} = \boldsymbol{R}_{3,i} = \mathrm{Rot}\left(z, -\pi/2 + 2\pi(i\text{-}1)/3\right)\mathrm{Rot}\left(x_{0,i}, \frac{\pi}{2}\right) = \left[\boldsymbol{u}_{0,i} \quad \boldsymbol{v}_{0,i} \quad \boldsymbol{w}_{0,i}\right]$: the nominal orientation matrix of $\left\{{}^{0}B_i\right\}$ ($\left\{{}^{3}_{0'}A_i\right\}$) with respect to $\{O\}$ ($\{O'\}$) with $\boldsymbol{w}_{0,i}$ being the unit vector of the $z_{0,i}$ axis

$\boldsymbol{R}_{1,i} = \mathrm{Rot}\left(z_{0,i}, \theta_i\right)$: the nominal orientation matrix of $\left\{{}^{1}_{0}B_i\right\}$ with respect to $\left\{{}^{0}B_i\right\}$ with θ_i being the nominal angle of the R-joint, and $\boldsymbol{R}_{0,i}\boldsymbol{R}_{1,i} = \left[\boldsymbol{u}_{1,i} \quad \boldsymbol{v}_{1,i} \quad \boldsymbol{w}_{1,i}\right]$ with $\boldsymbol{u}_{1,i}$ being the nominal unit vector of the proximal link in the ith limb

$\Delta\boldsymbol{b}_i$ ($\Delta\boldsymbol{a}_i$): the position error vector of B_i (A_i) evaluated in $\{O\}$ ($\{O'\}$) , and

$\Delta\boldsymbol{e} = \Delta\boldsymbol{b}_i - \Delta\boldsymbol{a}_i = (\Delta e_{x,i} \quad \Delta e_{y,i} \quad \Delta e_{z,i})^{\mathrm{T}}$

$\boldsymbol{\theta}_{0,i} = \left(\Delta\alpha_{0,i} \quad \Delta\beta_{0,i} \quad 0\right)^{\mathrm{T}}$: the orientation error vector of $\left\{{}^{0}B_i\right\}$ relative to its own nominal frame

$\boldsymbol{\theta}_{1,i} = \left(0 \quad 0 \quad \Delta\theta_i\right)^{\mathrm{T}}$, $\Delta\theta_i$: the encoder offset (the home error) of the R-joint in the ith limb

$\boldsymbol{\theta}_{2,i} = \left(\Delta\alpha_{2,i} \quad \Delta\beta_{2,i} \quad 0\right)^{\mathrm{T}}$: the orientation error vector of $\left\{{}^{2}_{1}C_i\right\}$ relative to $\left\{{}^{1}_{0}B_i\right\}$

$\boldsymbol{\theta}_{3,i} = \left(\Delta\alpha_{3,i} \quad \Delta\beta_{3,i} \quad 0\right)^{\mathrm{T}}$: the orientation error vector of $\left\{{}^{3}_{0'}A_i\right\}$ relative to its own nominal frame

$\Delta\boldsymbol{\varepsilon}_{j,i}$: the orientation error vector of the jth distal link in the ith limb

$\Delta\boldsymbol{\varepsilon} = (\Delta\varepsilon_x \quad \Delta\varepsilon_y \quad \Delta\varepsilon_z)^{\mathrm{T}}$: the orientation error vector of $\{O'\}$ relative to $\{O\}$

Also, it is easy to prove that the following relationships hold

$$\boldsymbol{u}_{0,i} \times \boldsymbol{u}_{1,i} = \sin\theta_i \boldsymbol{w}_{0,i}\,,\ \boldsymbol{v}_{0,i} \times \boldsymbol{u}_{1,i} = -\cos\theta_i \boldsymbol{w}_{0,i}\,,\ \boldsymbol{w}_{0,i} \times \boldsymbol{u}_{1,i} = \boldsymbol{v}_{1,i} \tag{2}$$

Note that $\left\{{}^{2}_{1}C_i\right\}$ ($\left\{{}^{3}_{0'}A_i\right\}$) is placed in such a way that the length error, $\Delta c_{c,i}(\Delta c_{a,i})$, between centres of two S-joints are equally shared by each side. This arrangement allows addition and subtraction to be made between two loop closure vector equations associated with the ith limb in Eq.(1). Thus

$$\Delta \boldsymbol{r} + \Delta \boldsymbol{\varepsilon} \times \boldsymbol{a}_i = \Delta \boldsymbol{e}_i + \Delta L_i \boldsymbol{u}_{1,i} + L\left(\Delta \alpha_{0,i} \boldsymbol{u}_{0,i} + \Delta \beta_{0,i} \boldsymbol{v}_{0,i} + \Delta \theta_i \boldsymbol{w}_{0,i}\right) \times \boldsymbol{u}_{1,i} + \Delta \bar{l}_i \hat{\boldsymbol{l}}_i + l \Delta \bar{\varepsilon}_i \times \hat{\boldsymbol{l}}_i \tag{3}$$

$$\Delta \boldsymbol{\varepsilon} \times \boldsymbol{w}_{0,i} = \frac{\Delta \tilde{c}_i}{c} \boldsymbol{w}_{0,i} + \left(-\Delta \alpha_{03,i} \boldsymbol{v}_{0,i} + \Delta \beta_{03,i} \boldsymbol{u}_{0,i} - \Delta \alpha_{2,i} \boldsymbol{v}_{1,i} + \Delta \beta_{2,i} \boldsymbol{u}_{1,i}\right) + \frac{\Delta \tilde{l}_i}{c} \hat{\boldsymbol{l}}_i + \frac{l}{c} \Delta \tilde{\varepsilon}_i \times \hat{\boldsymbol{l}}_i \tag{4}$$

where

$$\Delta \bar{l}_i = \frac{\Delta l_{1,i} + \Delta l_{2,i}}{2}, \ \Delta \bar{\varepsilon}_i = \frac{\Delta \varepsilon_{1,i} + \Delta \varepsilon_{2,i}}{2},$$

$$\Delta \bar{\varepsilon}_i = \Delta \varepsilon_{1,i} - \Delta \varepsilon_{2,i}, \ \Delta \tilde{l}_i = \Delta l_{1,i} - \Delta l_{2,i}, \ \Delta \tilde{c}_i = \Delta c_{c,i} - \Delta c_{a,i}, \ \Delta \alpha_{03,i} = \Delta \alpha_{0,i} - \Delta \alpha_{3,i}, \ \Delta \beta_{03,i} = \Delta \beta_{0,i} - \Delta \beta_{3,i}$$

Then, taking dot product with $\hat{\boldsymbol{l}}_i$ on the both sides of Eq.(3) and (4), yields

$$\begin{gathered} \hat{\boldsymbol{l}}_i^{\mathrm{T}} \Delta \boldsymbol{r} + \left(\boldsymbol{a}_i \times \hat{\boldsymbol{l}}_i\right)^{\mathrm{T}} \Delta \boldsymbol{\varepsilon} = L \Delta \theta_i \hat{\boldsymbol{l}}_i^{\mathrm{T}} \boldsymbol{v}_{1,i} + \hat{\boldsymbol{l}}_i^{\mathrm{T}} \Delta \boldsymbol{e}_i + \Delta L_i \hat{\boldsymbol{l}}_i^{\mathrm{T}} \boldsymbol{u}_{1,i} + L\left(\sin \theta_i \Delta \alpha_{0,i} - \cos \theta_i \Delta \beta_{0,i}\right) \hat{\boldsymbol{l}}_i^{\mathrm{T}} \boldsymbol{w}_{0,i} + \Delta \bar{l}_i \\ \left(\boldsymbol{w}_{0,i} \times \hat{\boldsymbol{l}}_i\right)^{\mathrm{T}} \Delta \boldsymbol{\varepsilon} = \frac{\Delta \tilde{l}_i}{c} + \frac{\Delta \tilde{c}_i}{c} \hat{\boldsymbol{l}}_i^{\mathrm{T}} \boldsymbol{w}_{0,i} + \hat{\boldsymbol{l}}_i^{\mathrm{T}} \left(-\Delta \alpha_{03,i} \boldsymbol{v}_{0,i} + \Delta \beta_{03,i} \boldsymbol{u}_{0,i} - \Delta \alpha_{2,i} \boldsymbol{v}_{1,i} + \Delta \beta_{2,i} \boldsymbol{u}_{1,i}\right) \end{gathered} \tag{5}$$

Rewriting Eq.(5) in matrix form finally results in the linearized geometric error model of the Delta robot

$$\boldsymbol{A}_{rr} \Delta \boldsymbol{r} + \boldsymbol{A}_{r\varepsilon} \Delta \boldsymbol{\varepsilon} = \boldsymbol{B}_r \Delta \boldsymbol{p}_r \tag{6}$$

$$\boldsymbol{A}_{\varepsilon\varepsilon} \Delta \boldsymbol{\varepsilon} = \boldsymbol{B}_\varepsilon \Delta \boldsymbol{p}_\varepsilon \tag{7}$$

where

$$\boldsymbol{A}_{rr} = \begin{bmatrix} \hat{\boldsymbol{l}}_1 & \hat{\boldsymbol{l}}_2 & \hat{\boldsymbol{l}}_3 \end{bmatrix}^{\mathrm{T}}, \ \boldsymbol{A}_{r\varepsilon} = \begin{bmatrix} \boldsymbol{a}_1 \times \hat{\boldsymbol{l}}_1 & \boldsymbol{a}_2 \times \hat{\boldsymbol{l}}_2 & \boldsymbol{a}_3 \times \hat{\boldsymbol{l}}_3 \end{bmatrix}^{\mathrm{T}}, \ \boldsymbol{A}_{\varepsilon\varepsilon} = \begin{bmatrix} \boldsymbol{w}_{0,1} \times \hat{\boldsymbol{l}}_1 & \boldsymbol{w}_{0,2} \times \hat{\boldsymbol{l}}_2 & \boldsymbol{w}_{0,3} \times \hat{\boldsymbol{l}}_3 \end{bmatrix}^{\mathrm{T}},$$

$$\boldsymbol{B}_r = \begin{bmatrix} \boldsymbol{B}_{r,1} & & \\ & \boldsymbol{B}_{r,2} & \\ & & \boldsymbol{B}_{r,3} \end{bmatrix}, \ \Delta \boldsymbol{p}_r = \begin{pmatrix} \Delta \boldsymbol{p}_{r,1} \\ \Delta \boldsymbol{p}_{r,2} \\ \Delta \boldsymbol{p}_{r,3} \end{pmatrix}, \ \boldsymbol{B}_{r,i} = \begin{bmatrix} \hat{\boldsymbol{l}}_i^{\mathrm{T}} \boldsymbol{v}_{1,i} & \hat{\boldsymbol{l}}_i^{\mathrm{T}} & \hat{\boldsymbol{l}}_i^{\mathrm{T}} \boldsymbol{u}_{1,i} & \hat{\boldsymbol{l}}_i^{\mathrm{T}} \boldsymbol{w}_{0,i} \sin \theta_i & -\hat{\boldsymbol{l}}_i^{\mathrm{T}} \boldsymbol{w}_{0,i} \cos \theta_i & 1 \end{bmatrix},$$

$$\Delta \boldsymbol{p}_{r,i} = \begin{pmatrix} L \Delta \theta_i & \Delta \boldsymbol{e}_i^{\mathrm{T}} & \Delta L_i & L \Delta \alpha_{0,i} & L \Delta \beta_{0,i} & \Delta \bar{l}_i \end{pmatrix}^{\mathrm{T}}, \ \boldsymbol{B}_\varepsilon = \begin{bmatrix} \boldsymbol{B}_{\varepsilon,1} & & \\ & \boldsymbol{B}_{\varepsilon,2} & \\ & & \boldsymbol{B}_{\varepsilon,3} \end{bmatrix}, \ \Delta \boldsymbol{p}_\varepsilon = \begin{pmatrix} \Delta \boldsymbol{p}_{\varepsilon,1} \\ \Delta \boldsymbol{p}_{\varepsilon,2} \\ \Delta \boldsymbol{p}_{\varepsilon,3} \end{pmatrix},$$

$$\boldsymbol{B}_{\varepsilon,i} = \begin{bmatrix} 1 & \hat{\boldsymbol{l}}_i^{\mathrm{T}} \boldsymbol{w}_{0,i} & -\hat{\boldsymbol{l}}_i^{\mathrm{T}} \boldsymbol{v}_{0,i} & \hat{\boldsymbol{l}}_i^{\mathrm{T}} \boldsymbol{u}_{0,i} & -\hat{\boldsymbol{l}}_i^{\mathrm{T}} \boldsymbol{v}_{1,i} & \hat{\boldsymbol{l}}_i^{\mathrm{T}} \boldsymbol{u}_{1,i} \end{bmatrix},$$

$$\Delta \boldsymbol{p}_{\varepsilon,i} = \begin{pmatrix} \Delta \tilde{l}_i / c & \Delta \tilde{c}_i / c & \Delta \alpha_{03,i} & \Delta \beta_{03,i} & \Delta \alpha_{2,i} & \Delta \beta_{2,i} \end{pmatrix}^{\mathrm{T}}$$

Note that $\boldsymbol{A}_{rr}$ and $\boldsymbol{A}_{\varepsilon\varepsilon}$ are non-singular, Eq.(6) and (7) can be rewritten as

$$\Delta \boldsymbol{r} = \begin{bmatrix} \boldsymbol{A}_{rr}^{-1} \boldsymbol{B}_r & -\boldsymbol{A}_{rr}^{-1} \boldsymbol{A}_{r\varepsilon} \boldsymbol{A}_{\varepsilon\varepsilon}^{-1} \boldsymbol{B}_\varepsilon \end{bmatrix} \begin{pmatrix} \Delta \boldsymbol{p}_r \\ \Delta \boldsymbol{p}_\varepsilon \end{pmatrix} = \begin{bmatrix} \boldsymbol{C}_{rr} & \boldsymbol{C}_{r\varepsilon} \end{bmatrix} \begin{pmatrix} \Delta \boldsymbol{p}_r \\ \Delta \boldsymbol{p}_\varepsilon \end{pmatrix} = \boldsymbol{C}_r \Delta \boldsymbol{p} \tag{8}$$

$$\Delta \boldsymbol{\varepsilon} = \boldsymbol{A}_{\varepsilon\varepsilon}^{-1} \boldsymbol{B}_\varepsilon \Delta \boldsymbol{p}_\varepsilon = \boldsymbol{C}_\varepsilon \Delta \boldsymbol{p}_\varepsilon \tag{9}$$

Examination of Eqs.(8) and (9) shows that there are 18 geometric source errors, $\Delta \boldsymbol{p}_{\varepsilon}$, in total affecting the angular accuracy of the traveling plate, so this model is named the model 18; and there are 42 geometric source errors, $\Delta \boldsymbol{p}_{r}$ and $\Delta \boldsymbol{p}_{\varepsilon}$, affecting the positioning accuracy of the reference point, so the corresponding model is called the model 42. Obviously, $\Delta \boldsymbol{p}_{\varepsilon}$ should be eliminated or at least minimized in manufacturing and assembly process as $\Delta \boldsymbol{\varepsilon}$ caused by $\Delta \boldsymbol{p}_{\varepsilon}$ is uncompensatable in nature. By assuming the traveling plate perfectly parallel to the base frame, the number of world coordinates can then be reduced to 3 Cartesian coordinates in terms of position of any point on the traveling plate. This simplification requires not only that the $z_{0,i}$, $z_{2,i}$ and $z_{3,i}$ axes remain perfectly parallel to each other as remarked in [7] but also that the length discrepancies $\Delta \tilde{l}_i$ and $\Delta \tilde{c}_i$ vanish. Consequently, Eq.(8) can be reduced to the model containing 24 source errors (known as the model 24) as follows

$$\Delta \boldsymbol{r} = \boldsymbol{A}_{rr}^{-1} \boldsymbol{B}_{r} \Delta \boldsymbol{p}_{r} \tag{10}$$

3. Source Error Identification

In this section we will develop two models for source error identification using the distance-based approach. The first model is developed using Eq.(10) and the second model is developed using Eq.(8). We will make an in-depth discussion on the source error identifiability of the second model.

3.1 Identification model using distance measurements

As shown in Fig. 3, the position vector of the reference point P on the traveling plate with regard to the world frame $\{O_w\}$ can be decomposed into two components, i.e. the position vector of the point relative to the base frame $\{O\}$ and that of O relative to $\{O_w\}$. Note that the distance between two

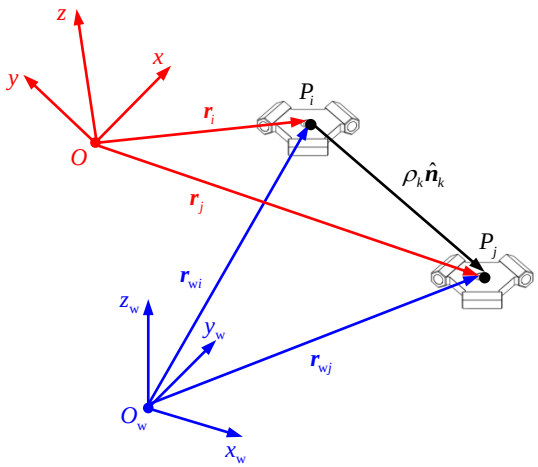

Fig. 3 The principle of the distance measurement

positions of a same point is invariant with the frame chosen. This property allows the source errors to be identified using distance measurements as long as $\{O\}$ is specified by eliminating the rigid body motion of $\{O\}$ relative to $\{O_w\}$. Then, robot localization needs to be made according to the environment context. For this reason, we may assume that the following source errors vanish though there are many other possible choices.

$$\Delta e_{x,1} = 0\,,\ \Delta e_{y,2} = \Delta e_{y,3} = 0\,,\ e_{z,1} = \Delta e_{z,2} = \Delta e_{z,3} = 0 \tag{11}$$

This treatment results in the model containing 18 source errors (known as the model 18) in the form of Eq.(10), and the model containing 36 source errors (known as the model 36) in the form of Eq.(8). Building upon the above assumption, we use two different positions P_i to P_j ($i \neq j$) of the reference point *P* to form a measuring pair numbered by *k* as shown Fig. 3. Thus, the corresponding loop closure equation can be expressed as

$$\rho_k \hat{\boldsymbol{n}}_k = \boldsymbol{r}_j - \boldsymbol{r}_i \tag{12}$$

where ρ_k and $\hat{\boldsymbol{n}}_k$ denote the magnitude and unit vector of $\overrightarrow{P_iP_j}$, $\boldsymbol{r}_{i(j)}$ denotes the position vector of P_i (P_j). Taking the first-order approximation of Eq.(12), yields

$$\begin{gathered}\Delta\rho_k \hat{\boldsymbol{n}}_{0k} + \rho_{0k}\Delta\hat{\boldsymbol{n}}_k \approx \Delta\boldsymbol{r}_j - \Delta\boldsymbol{r}_i \approx \begin{bmatrix}\tilde{\boldsymbol{C}}_{rr,k} & \tilde{\boldsymbol{C}}_{r\varepsilon,k}\end{bmatrix}\begin{pmatrix}\Delta\boldsymbol{p}_r \\ \Delta\boldsymbol{p}_\varepsilon\end{pmatrix} \\ \tilde{\boldsymbol{C}}_{rr,k} = \boldsymbol{C}_{rr,j} - \boldsymbol{C}_{rr,i}\,,\ \ \tilde{\boldsymbol{C}}_{r\varepsilon,k} = \boldsymbol{C}_{r\varepsilon,j} - \boldsymbol{C}_{r\varepsilon,i}\end{gathered} \tag{13}$$

where ρ_{0k} and $\hat{\boldsymbol{n}}_{0k}$ denote the nominal magnitude and unit vector of $\overrightarrow{P_iP_j}$. Then, taking dot product with $\hat{\boldsymbol{n}}_{0k}$ on both sides of Eq.(13), gives

$$\Delta\rho_k = \hat{\boldsymbol{n}}_{0k}^{\mathrm{T}}\begin{bmatrix}\tilde{\boldsymbol{C}}_{rr,k} & \tilde{\boldsymbol{C}}_{r\varepsilon,k}\end{bmatrix}\begin{pmatrix}\Delta\boldsymbol{p}_r \\ \Delta\boldsymbol{p}_\varepsilon\end{pmatrix} = \begin{bmatrix}\boldsymbol{h}_{r,k} & \boldsymbol{h}_{\varepsilon,k}\end{bmatrix}\begin{pmatrix}\Delta\boldsymbol{p}_r \\ \Delta\boldsymbol{p}_\varepsilon\end{pmatrix},\ k = 1, 2, \cdots, K \tag{14}$$

Hence, the matrix form of Eq.(14) for the model 18 and the model 36 can be expressed respectively as

$$\Delta\boldsymbol{\rho} = \boldsymbol{H}_r \Delta\boldsymbol{p}_r \tag{15}$$

$$\Delta\boldsymbol{\rho} = \begin{bmatrix}\boldsymbol{H}_r & \boldsymbol{H}_\varepsilon\end{bmatrix}\begin{pmatrix}\Delta\boldsymbol{p}_r \\ \Delta\boldsymbol{p}_\varepsilon\end{pmatrix} = \boldsymbol{H}\Delta\boldsymbol{p} \tag{16}$$

where

$$\boldsymbol{H}_r = \begin{pmatrix}\boldsymbol{h}_{r,1} \\ \vdots \\ \boldsymbol{h}_{r,K}\end{pmatrix},\ \boldsymbol{H}_\varepsilon = \begin{pmatrix}\boldsymbol{h}_{\varepsilon,1} \\ \vdots \\ \boldsymbol{h}_{\varepsilon,K}\end{pmatrix},\ \Delta\boldsymbol{\rho} = \begin{pmatrix}\Delta\rho_1 \\ \vdots \\ \Delta\rho_K\end{pmatrix}$$

3.2 Identifiability analysis

Having two error models given in Eq.(15) and (16) to hand, the source error identifiability will be investigated. For the model 18, it is easy to prove that $\Delta\boldsymbol{p}_r$ is identifiable if $\text{rank}(\boldsymbol{H}_r)=18$. This condition can be fulfilled by letting the traveling plate undergo all controllable poses and the number of distance measurements of a single point on the traveling plate satisfies $K\geq 18$. Thus, the linear least square estimation gives

$$\Delta\boldsymbol{p}_r=\boldsymbol{H}_r^{+}\Delta\boldsymbol{\rho} \tag{17}$$

Particularly, assume the positioning errors of the reference point P is merely caused by the encoder offsets, $\Delta\boldsymbol{p}_r$ is identifiable if $K\geq 3$ provided that the selected poses, e.g. $\boldsymbol{r}_1$, $\boldsymbol{r}_2$ and $\boldsymbol{r}_3$ .are not co-linear.

For the model 36, however, the row-echelon form of $\boldsymbol{H}$ shows that $\text{rank}(\boldsymbol{H})\equiv 32$, even if the travelling plate undergoes all controllable configurations and the number of distance measurements of three non-coplanar points on the travelling plate satisfies $K\geq 36$. This means that there are four source errors in $\Delta\boldsymbol{p}_\varepsilon$ that cannot be identified by the distance-based approach. In order to gain a deep insight into this interesting phenomenon, examine any row vector $\boldsymbol{h}=\begin{bmatrix}\boldsymbol{h}_r & \boldsymbol{h}_\varepsilon\end{bmatrix}$ of $\boldsymbol{H}$ by omitting its subscript *k* for the time being

$$\boldsymbol{h}_r=\begin{bmatrix}\boldsymbol{h}_{r,1} & \boldsymbol{h}_{r,2} & \boldsymbol{h}_{r,3}\end{bmatrix},\ \boldsymbol{h}_\varepsilon=\begin{bmatrix}\boldsymbol{h}_{\varepsilon,1} & \boldsymbol{h}_{\varepsilon,2} & \boldsymbol{h}_{\varepsilon,3}\end{bmatrix} \tag{18}$$

where the entries $h_{r,i,2},\ldots,h_{r,i,6}$ in $\boldsymbol{h}_{r,i}$ correspond to $L\Delta\theta_{1,i}$, ΔL_i, $L\Delta\alpha_{0,i}$, $L\Delta\beta_{0,i}$, $\Delta\bar{l}_i$ in $\Delta\boldsymbol{p}_{r,i}$ ($i=1,2,3$), the entries $h_{\varepsilon,i,1},\ldots,h_{\varepsilon,i,6}$ in $\boldsymbol{h}_{r,i}$ correspond to $\Delta\tilde{l}_i/c$, $\Delta\tilde{c}_i/c$, $\Delta\alpha_{03,i}$, $\Delta\beta_{03,i}$, $\Delta\alpha_{2,i}$, $\Delta\beta_{2,i}$ in $\Delta\boldsymbol{p}_{\varepsilon,i}$ ($i=1,2,3$), and the entries $h_{r,1,1}$, $h_{r,2,1}$, $h_{r,3,1}$ correspond to $\Delta e_{y,1}$, $\Delta e_{x,2}$, $\Delta e_{x,3}$, respectively. Again, the row-echelon form of $\boldsymbol{H}$ shows that four out of nine entries $h_{\varepsilon,i,3},h_{\varepsilon,i,4},h_{\varepsilon,i,5}$ ($i=1,2,3$), i.e., two out of three $h_{\varepsilon,i,3}$, one out of three $h_{\varepsilon,i,4}$, and one out of three $h_{\varepsilon,i,5}$ ($i=1,2,3$), are linearly dependent of $h_{r,i,2}$, $h_{r,i,4}$ and $h_{r,i,5}$. For the specified base frame, these linear relationships can be formulated by

$$\begin{aligned}
h_{\varepsilon,2,3}-h_{\varepsilon,1,3}&=\frac{La}{e}\left(\frac{1}{\sqrt{3}}\left(\left(h_{r,3,2}-h_{r,1,2}\right)+\left(h_{r,3,2}-h_{r,2,2}\right)\right)+\left(h_{r,2,4}-h_{r,1,4}\right)\right)\\
h_{\varepsilon,3,3}-h_{\varepsilon,1,3}&=\frac{La}{e}\left(-\frac{1}{\sqrt{3}}\left(\left(h_{r,2,2}-h_{r,1,2}\right)+\left(h_{r,2,2}-h_{r,3,2}\right)\right)+\left(h_{r,3,4}-h_{r,1,4}\right)\right)\\
\frac{L}{e}\sum_{i=1}^{3}h_{\varepsilon,i,5}+3h_{\varepsilon,1,3}&=\frac{La}{e}\sqrt{3}\left(\sqrt{3}h_{r,1,4}+h_{r,2,2}-h_{r,3,2}\right)\\
\sum_{i=1}^{3}h_{\varepsilon,1,4}&=\frac{La}{e}\sum_{i=1}^{3}h_{r,1,5}
\end{aligned} \tag{19}$$

where $e = b - a$ with b and a being radii of the nominal equilateral triangles $\Delta B_1 B_2 B_3$ and $\Delta A_1 A_2 A_3$. In this sense, $\boldsymbol{h}_\varepsilon$ should be degenerated by removing the entries corresponding to $\Delta\alpha_{03,2}$, $\Delta\alpha_{03,3}$, $\Delta\beta_{03,3}$, $\Delta\alpha_{2,3}$ for instance, reducing the model 36 to the model 32. Hence, by assuming again that the traveling plate undergoes all controllable configurations and the number of distance measurements of at least two points on the traveling plate satisfies $K \geq 32$, the remaining source errors can be identified using the linear last square method

$$\Delta \boldsymbol{p} = \boldsymbol{H}^{+} \Delta \boldsymbol{\rho} \tag{20}$$

It should be pointed out that although the source errors affecting the angular pose accuracy cannot fully be identified by the distance-based method, the positioning errors induced by the realistic unidentifiable source errors can partially be compensated because these errors are shared amongst the identifiable ones *via* the least square algorithm.

3.3 Optimal pose selection

In the implementation of kinematic calibration of the Delta robot, choosing a set of optimal poses is an important issue to ensure the measurement efficiency and the identification accuracy. The straightforward and reasonable way to do so is to choose n evenly spaced poses on each of two layers of the cylindrical workspace boundary as shown in Fig.4.

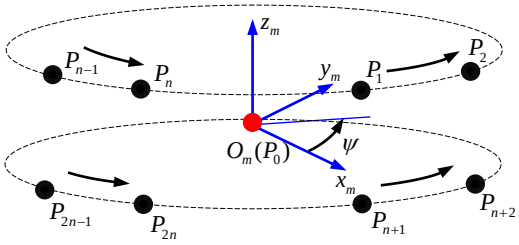

Fig.4 Measurement pose selection

This is because: (1) the necessary condition for the full set of source errors to be identifiable requires the travelling plate to experience all controllable degrees of freedom of the system (i.e. three translations in the case) [19], and (2) the optimal poses tend to converge to the workspace boundary [20] where the highest signal/noise ratio can be achieved. Together with the reference pose P_0 at the centre of the cylindrical workspace, these considerations result in $2n+1$ poses, leading to $K = C_{2n+1}^2 = n(2n+1)$ distance measurements generated by the combinations of all the possible pairs of these poses. Since the condition number κ of the identification matrix $\boldsymbol{H}$ monotonously decreases

with the increase of the number of measurement poses n [21], the problem of the pose optimization can then be resolved by minimizing n subject to a given threshold ε_0 defined as the relative differentiation of $\kappa_n = \kappa\left(\boldsymbol{H}(n)\right)$ *vs.* n, i.e.

$$\begin{cases} \min n \\ \text{s.t.} \quad \varepsilon = \dfrac{\left|\kappa_n - \kappa_{n-1}\right|}{\kappa_n} \times 100\% \le \varepsilon_0 \\ n \ge 3 \end{cases} \tag{21}$$

4. Error Compensation

4.1 Linear compensator design

Once the source errors have been estimated by the method given in Section 3, a linear error compensator can be designed. For the model 32, this can be done by adding an additional term $\boldsymbol{B}_m \Delta \boldsymbol{q}_m$ to the right hand of Eq.(8) such that

$$\boldsymbol{A}_{rr} \Delta \boldsymbol{r} = \boldsymbol{B}_r \Delta \boldsymbol{p}_r - \boldsymbol{A}_{r\varepsilon} \boldsymbol{A}_{\varepsilon\varepsilon}^{-1} \boldsymbol{B}_\varepsilon \Delta \boldsymbol{p}_\varepsilon + \boldsymbol{B}_m \Delta \boldsymbol{q}_m \tag{22}$$

$$\Delta \boldsymbol{q}_m = L \Delta \boldsymbol{\theta}_m, \ \Delta \boldsymbol{\theta}_m = \begin{pmatrix} \Delta\theta_{m,1} & \Delta\theta_{m,2} & \Delta\theta_{m,3} \end{pmatrix}^{\mathrm{T}}, \ \boldsymbol{B}_m = \begin{bmatrix} \hat{\boldsymbol{l}}_1^{\mathrm{T}} \boldsymbol{v}_{1,1} & & \\ & \hat{\boldsymbol{l}}_2^{\mathrm{T}} \boldsymbol{v}_{2,1} & \\ & & \hat{\boldsymbol{l}}_3^{\mathrm{T}} \boldsymbol{v}_{3,1} \end{bmatrix}$$

where $\Delta\theta_{m,i}$ is regarded as the encoder offset compensator of the actuated R-joint in the ith limb. It is easy to see that the necessary condition to force the term $\boldsymbol{B}_r \Delta \boldsymbol{p}_r - \boldsymbol{A}_{r\varepsilon} \boldsymbol{A}_{\varepsilon\varepsilon}^{-1} \boldsymbol{B}_\varepsilon \Delta \boldsymbol{p}_\varepsilon + \boldsymbol{B}_m \Delta \boldsymbol{q}_m$ to be a zero vector is that $\Delta \boldsymbol{r} \equiv \boldsymbol{0}$ since $\boldsymbol{A}_{rr}$ is non-singular. This consideration leads to the development of a linear error compensator that can be represented by

$$\Delta \boldsymbol{q}_m = -\boldsymbol{B}_m^{-1} \left(\boldsymbol{B}_r \Delta \boldsymbol{p}_r - \boldsymbol{A}_{r\varepsilon} \boldsymbol{A}_{\varepsilon\varepsilon}^{-1} \boldsymbol{B}_\varepsilon \Delta \boldsymbol{p}_\varepsilon \right) \tag{23}$$

It can also be seen from Eq.(22) that $\Delta \boldsymbol{q}_m$ is a function of the source errors, nominal dimensions and configuration of the robot, and it can be generated with ease for real-time error compensation since the explicit expression of $\boldsymbol{A}_{\varepsilon\varepsilon}^{-1}$ can be achieved by

$$\boldsymbol{A}_{\varepsilon\varepsilon}^{-1} = \frac{1}{\boldsymbol{n}_1^{\mathrm{T}} \left(\boldsymbol{n}_2 \times \boldsymbol{n}_3 \right)} \begin{bmatrix} \boldsymbol{n}_2 \times \boldsymbol{n}_3 & \boldsymbol{n}_3 \times \boldsymbol{n}_1 & \boldsymbol{n}_1 \times \boldsymbol{n}_2 \end{bmatrix}^{\mathrm{T}}, \ \boldsymbol{n}_i = \boldsymbol{w}_{0,i} \times \hat{\boldsymbol{l}}_i \tag{24}$$

For the model 18, $\Delta \boldsymbol{q}_m$ can simply be formulated by

$$\Delta \boldsymbol{q}_m = -\boldsymbol{B}_m^{-1} \boldsymbol{B}_r \Delta \boldsymbol{p}_r \tag{25}$$

4.2 Error compensation strategy

Considering that the positioning errors caused by the encoder offsets (at 1-5 millimetre level) are much larger than those caused by the other source errors (at 1/5 millimetre level or less), the parameter identification and error compensation can be implemented by two steps to reduce the cut-off errors arising from the linearization.

Step 1: Encoder offset compensation

Assume that the positioning errors of the reference point P is merely caused by the encoder offsets. Then, Eq.(8) can be degenerated into the form

$$\Delta \boldsymbol{r} = \boldsymbol{A}_{rr}^{-1}\boldsymbol{B}_m \Delta \boldsymbol{p}_\theta ,\ \Delta \boldsymbol{p}_\theta = L\Delta \boldsymbol{\theta} ,\ \Delta \boldsymbol{\theta} = \begin{pmatrix} \Delta\theta_1 & \Delta\theta_2 & \Delta\theta_3 \end{pmatrix}^{\mathrm{T}} \tag{26}$$

Hence, equipped with at least three distance measurements to hand, the encoder offsets can roughly be identified using Eq.(17) and thereby the positioning error of P can roughly be compensated in an iterative manner until the estimated source errors converge to a specified threshold.

Step 2: Fine (full) error compensation .

On the basis of Step 1, fine identification and error compensation can be carried out by taking into account full/partial source errors using either the model 32 or the model 18, depending upon the orientation accuracy of the traveling plate.

5. Experimental Verification

In order to verify the effectiveness of the calibration method proposed in this article, experiments are carried out on a prototype Delta robot having the repeatability of ± 0.05 mm over its cylindrical task workspace. The nominal geometric parameters of the Delta robot and the dimensions of its cylindrical task workspace are given in Table 1, where H denotes the distance from the *x-y* plane to the top layer of the workspace, and R and h denote the radius and height of the workspace as shown in Fig. 2.

Since the distance errors before encoder offset calibration may be beyond the measuring range of a double ball bar, a LEICA AT901-LR laser tracker with the maximum observed deviation of 0.005 mm is employed to measure the coordinates of the reference point P (i.e. the centre of sphere reflector) at different configurations, and each measurement is repeated three times, and only the mean values are retained. Having built the experiment set-up shown in Fig. 5, the procedures for the rough (encoder offset) and fine calibrations are addressed in what follows.

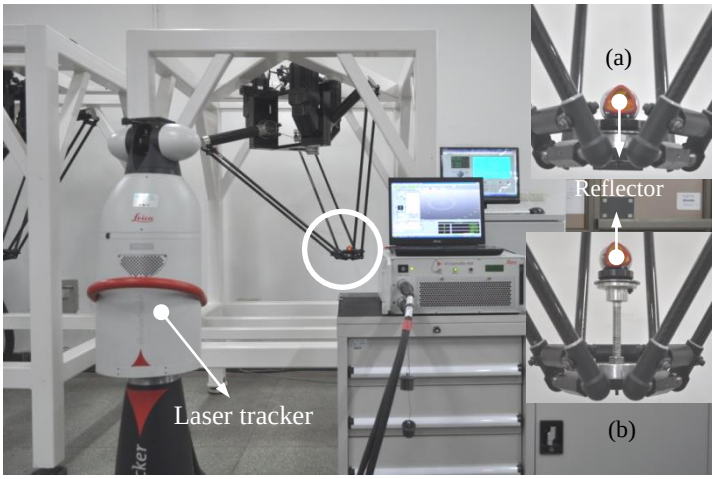

Fig. 5 The experiment set-up

Table 1 Nominal geometric parameters of the prototype Delta robot (unit：mm)

b	a	L	l	c	H	R	h
200	51	375	950	100	728	500	250

5.1 Rough (encoder offset) calibration

In the rough calibration, assume that the point P undergoes $n \geq 3$ evenly spaced poses along the boundary of middle layer of the workspace since $\Delta \boldsymbol{p}_\theta$ is identifiable if $K \geq 3$ provided that the three selected poses are not co-linear. Given the threshold $\varepsilon_0 = 1\%$, it is easy to see that the minimum number of the measurement poses is $n = 5$ as shown in Fig.6. Therefore, evaluated in the virtual frame $\{O_m\}$ established by the laser tracker, the realistic coordinates of P at the above poses are measured, resulting in $K = C_6^2 = 15$ distance errors generated by the coordinate measurements. Consequently, the encoder offsets, $\Delta \boldsymbol{p}_\theta$, can be roughly identified using Eq.(17) and the positioning errors of P caused by the estimated $\Delta \boldsymbol{p}_\theta$ can be compensated using Eq.(25) . In the experiment, we need to run the calibration procedure twice due to the relatively large encoder offsets until they converge to $\Delta\theta_1 = 0.911^\circ$, $\Delta\theta_2 = 1.098^\circ$ and $\Delta\theta_3 = 1.441^\circ$. It can be seen from Table 2 that the maximum distance error denoted by $\Delta\rho$ and the maximum volumetric error denoted by Δv of the P_k ($k = 1,2,\ldots,5$) relative to P_0 can dramatically be reduced from 4.181mm and 4.962 mm to 0.187 mm and 1.047 mm, respectively, *via* the encoder offset calibration.

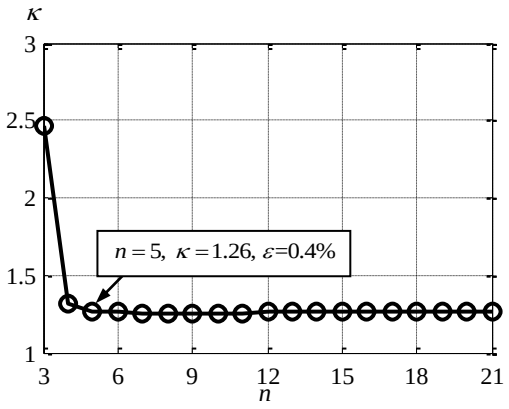

Fig.6 The variations of κ *vs.* n in the rough calibration

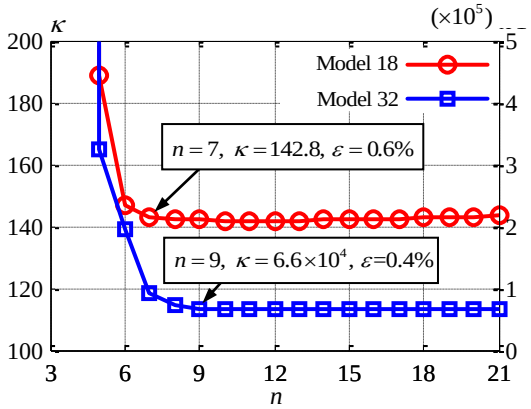

Fig.7 The variations of κ *vs.* n in the find calibration

Table 2 Distance and volumetric errors before and after encoder offset compensation (unit: mm)

Points		P_1	P_2	P_3	P_4	P_5
Before	$\Delta\rho$	-3.405	-3.859	-2.863	-4.181	-2.663
	Δv	3.769	3.888	3.163	4.962	2.975
After	$\Delta\rho$	0.025	-0.061	0.008	0.187	-0.011
	Δv	0.309	1.015	0.961	0.859	1.047

5.2 Fine calibration

In the fine calibration, the model 18 and model 32 are used respectively to investigate their difference in terms of the end results of calibration. According to Section 3.3, assume that the point P undergoes $n \geq 4$ evenly spaced poses along the boundary of top and bottom layers of the workspace. Given $\varepsilon_0 = 1\%$ again, it can be seen from Fig.7 that the minimum number of the measurement poses is $n = 7$ for the model 18 and $n = 9$ for the model 32. Therefore, for the model 18, $K = C_{15}^2 = 105$ distance errors can be generated using the coordinate measurements of P, i.e. the reflector centre as shown in Fig. 5(a), at $2n+1 = 15$ poses to identify $\Delta\boldsymbol{p}_r$. In the experiment, we only need to run the calibration procedure once for identifying $\Delta\boldsymbol{p}_r$ because sufficient accuracy can be achieved thanks to the encoder offset calibration ahead. As a result, $\Delta\boldsymbol{p}_r$ are identified as represented in Table 3. The difference in calibration procedure using the model 32 from that using the model 18 lies in that two sets of distance errors are needed for identifying both $\Delta\boldsymbol{p}_r$ and $\Delta\boldsymbol{p}_\varepsilon$. The first set corresponds to the reference point shown in Fig. 5(a), and the second set relates the reference point shown in Fig. 5(b) because the orientation errors of the travelling plate about the x and y axes can be detected by this arrangement. Thus, for the model 32, $K = 2C_{19}^2 = 342$ distance errors can be generated using the

coordinate measurements of the P at $2n+1=19$ poses, allowing $\Delta\boldsymbol{p}$ to be identified using Eq.(20) as represented in Table 4.

To evaluate robot accuracy after calibration, coordinate measurements on the circles of radii 250 mm and 500 mm in the top, middle and bottom layers are taken. This makes a total of 96 poses beside the home configuration. Each validation measurement is repeated three times, and the mean values are retained. Then, the distance and volumetric errors at all the poses relative to the home pose can be calculated. As represented in Table 5, by using the compensator given in Eq.(25) for the model 18, the maximum absolute distance error and the maximum volumetric error (after encoder offset calibration) are reduced from 0.682 mm and 1.303 mm to 0.167 mm and 0.386 mm; whereas by using the compensator given in Eq.(23) for the model 32, the corresponding errors are reduced to 0.134 mm and 0.371 mm, respectively. Given R= 500 mm in the middle layer of the workspace, Fig.8 shows the variations of the distance and volumetric errors *vs.* the swing angel Ψ (see Fig.4) before and after fine calibration. It can be seen that the variations for the model 18 differ from those for the model 32, but the positioning accuracy can slightly be improved by the model 32. This implies that the source errors affecting the uncompensatable pose accuracy have been well suppressed in building that robot, these source errors thereby have little bearing on the end results of kinematic calibration.

Table 3 Results of source error identification using the model 18 (unit：mm)

	$\Delta e_{x,i}$	$\Delta e_{y,i}$	$L\Delta\theta_i$	ΔL_i	$L\Delta\alpha_{0,i}$	$L\Delta\beta_{0,i}$	$\Delta\bar{l}_i$
Limb 1	--	0.114	0.965	0.112	-0.841	0.421	0.107
Limb 2	-0.201	--	-0.034	0.101	-0.546	-0.764	0.157
Limb 3	0.146	--	-0.578	0.098	0.759	0.432	0.302

Table 4 Results of source error identification using the model 32 (unit：mm)

	$\Delta e_{x,i}$	$\Delta e_{y,i}$	$L\Delta\theta_i$	ΔL_i	$L\Delta\alpha_{0,i}$	$L\Delta\beta_{0,i}$	$\Delta\bar{l}_i$
Limb 1	--	0.160	1.107	0.919	-0.707	0.636	0.114
Limb 2	-0.187	--	-0.112	0.110	-0.901	-0.524	0.125
Limb 3	0.174	--	-0.941	0.122	0.872	0.497	0.193
	$\Delta\tilde{l}_i$	$\Delta\tilde{c}_i$	$c\Delta\alpha_{03,i}$	$c\Delta\beta_{03,i}$	$c\Delta\alpha_{2,i}$	$c\Delta\beta_{2,i}$	
Limb 1	0.048	-0.021	-0.175	0.267	0.057	-0.032	
Limb 2	0.052	0.014	--	-0.242	-0.017	-0.047	
Limb 3	0.039	-0.009	--	--	--	0.061	

Table 5 The maximum distance and volumetric errors over the task workspace before and after calibration

	A		B		C_{18}		C_{32}	
	$\Delta\rho$	Δv	$\Delta\rho$	Δv	$\Delta\rho$	Δv	$\Delta\rho$	Δv
Max.	5.704	6.361	0.682	1.303	0.167	0.386	0.134	0.371

A—Before encoder offset calibration, B—After encoder offset calibration, C_{18} —Model 18-based calibration, C_{32} —Model 32-based calibration.

6. Conclusions

This paper investigates the kinematic calibration of Delta robot using distance based approach and the following conclusions are drawn:

(1) We have developed two linear models for kinematic calibration of the Delta robot. The model 18 can be used to identify the source errors affecting the positioning accuracy whereas the model 32 can be employed to identify a partial set of source errors affecting both the positioning and orientation errors of the travelling plate.

(2) We have found that the errors identified by the model 18 are different from the same set identified by the model 32 due to the unmodelled errors. We have also found that although the source errors affecting the orientation accuracy of the travelling plate cannot fully be identified by the distance-based approach, the positioning errors induced by the realistic unidentifiable source errors can still partially be compensated because these errors are shared amongst the identifiable ones *via* the least square algorithm.

(3) We strongly recommend the model 18 to be used in practice provided that the source errors affecting the uncompensatable (angular) pose accuracy can be eliminated or at least minimized *via* tolerance design, manufacturing as well as assembly processes.

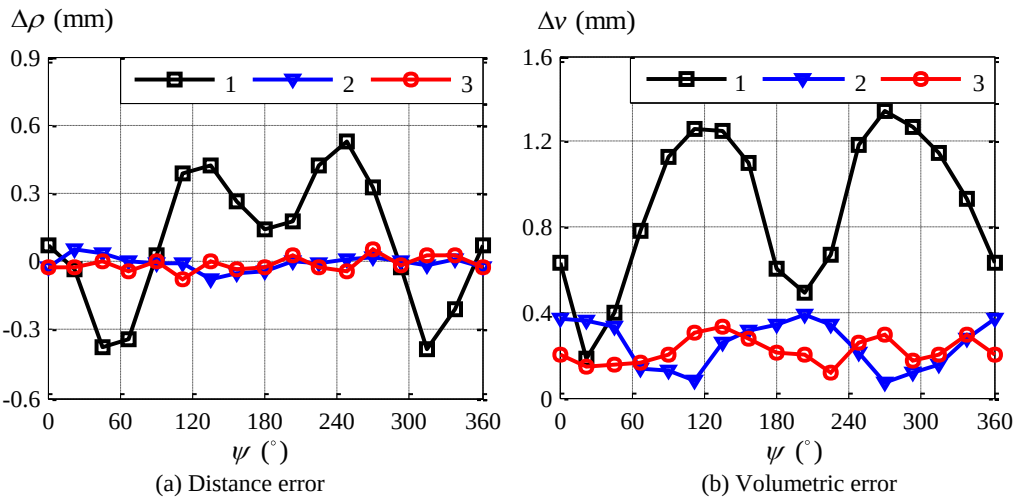

(a) Distance error (b) Volumetric error

Fig. 8 Distance and volumetric errors before and after the calibration across the middle layer in the workspace. (1: Before fine calibration; 2: Calibration using the model 18; 3: Calibration using the model 32)

Acknowledgements

This work is partially supported by the National Natural Science Foundation of China (NSFC) under grant 51135008, The Talent Introduction and Technology Development Program of Tianjin under grant 13RCHZGX01118, and The Tianjin Technical Innovation Funds for the Small Sci-tech Enterprises under grant 14C26211200362.

References

1. Roth ZS, Mooring B and Ravani B. An overview of robot calibration. *Int J Robot Autom* 1987; 3: 377-385.
2. Elatta A, Gen LP, Zhi FL, et al. An overview of robot calibration. *Information Technology Journal* 2004; 3: 74-78.
3. Majarena AC, Santolaria J, Samper D, et al. An overview of kinematic and calibration models using internal/external sensors or constraints to improve the behavior of spatial parallel mechanisms. *Sensors-Basel* 2010; 10: 10256-10297.
4. Iura cu CC and Park FC. Geometric algorithms for kinematic calibration of robots containing closed loops. *J Mech Design* 2003; 125: 23-32.
5. Zhuang H, Masory O and Yan J. Kinematic calibration of a Stewart platform using pose measurements obtained by a single theodolite. In: *Proceedings of the IEEE/RSJ International Conference on Intelligent Robots and Systems (IROS)*, Pittsburgh, Pennsylvania, 5-9 August 1995, pp. 329-34.
6. Maurine P and Dombre E. A calibration procedure for the parallel robot Delta 4. In: *Proceedings of the IEEE International Conference on Robotics and Automation (ICRA)*, Minneapolis, Minnesota, 22-28 April 1996, pp. 975-982.
7. Vischer P and Clavel R. Kinematic calibration of the parallel Delta robot. *Robotica* 1998; 16: 207-218.
8. Deblaise D and Maurine P. Effective geometrical calibration of a delta parallel robot used in neurosurgery. In: *Proceedings of the IEEE/RSJ International Conference on Intelligent Robots and Systems (IROS)*, Alberta, Canada, 2-6 August 2005, pp. 1313-1318.
9. Corbel D, Nabat V and Maurine P. Geometrical Calibration of the High Speed Robot Par4 Using a Laser Tracker. In: *Proceedings of the International Conference on Methods and Models in Automation and Robotics (MMAR)*, Miedzyzdroje, Poland, 28-31 August 2006, pp. 687-692.
10. Khalil W and Besnard S. Self calibration of Stewart-Gough parallel robots without extra sensors. *IEEE Trans on Robot Autom* 1999; 15: 1116-1121.
11. Last P, Budde C and Hesselbach J. Self-calibration of the HEXA-parallel-structure. In: *Proceedings of the*

IEEE International Conference on Automation Science and Engineering(CASE), Edmonton, Canada, 1-2 August 2005, pp. 393-398.

12. Zhu Y, Yan J, Zhao J, et al. Autonomous kinematic self-calibration of a novel haptic device. In: *Proceedings of the IEEE/RSJ International Conference on Intelligent Robots and Systems (IROS)*, Beijin, China, 9-15 October 2006, pp. 4654-4659.
13. Meng Y and Zhuang H. Autonomous robot calibration using vision technology. *Robot Cim-Int Manuf* 2007; 23: 436-446.
14. Clavel R, Device for the movement and positioning of an element in space, Patent 4976582, USA, 1990.
15. Lintott A and Dunlop G. Parallel topology robot calibration. *Robotica* 1997; 15: 395-398.
16. Ecorchard G and Maurine P. Self-calibration of Delta parallel robots with elastic deformation compensation. In: *Proceedings of the IEEE/RSJ International Conference on Intelligent Robots and Systems (IROS)*, Alberta, Canada, 2-6 August 2005, pp. 462-467.
17. Renaud P, Andreff N, Lavest J-M, et al. Simplifying the kinematic calibration of parallel mechanisms using vision-based metrology. *IEEE Trans Robot* 2006; 22(1): 12-22.
18. Savoure L, Maurine P, Corbel D, et al. An improved method for the geometrical calibration of parallelogram-based parallel robots. In: *Proceedings of the IEEE International Conference on Robotics and Automation (ICRA)*, Orlanda, Florida, USA, 15-19 May 2006, pp. 769-776.
19. Huang T, Chetwynd D, Whitehouse D, et al. A general and novel approach for parameter identification of 6-DOF parallel kinematic machines. *Mech Mach Theory* , 2005, 40(2): 219-239.
20. Daney D, Madeline B and Papegay Y. Choosing measurement poses for robot calibration with local convergence method and tabu search. *Int J Robot Res*, 2005, 24(6): 501-518.
21. Driels M and Pathre U. Significance of observation strategy on the design of robot calibration experiments, *J Robot Syst*, 1990, 7(2): 197-223.